Supporting Information

Precision Ladder-Structured Silver Cluster Assembly Bridged by Tetrazine Linkers for Highly Sensitive and Selective Luminescence Recognition of Amino Acids

Tsukasa Irie,[a†] *Riki Nakatani,*[a†] *Sreelakshmi K. S.,*[a] *Ayumu Kondo,*[a] *Tokuhisa Kawawaki,*[a] *Shuntaro Takahashi,*[b] *Saikat Das**[a] *and Yuichi Negishi**[a]

[a]Institute of Multidisciplinary Research for Advanced Materials, Tohoku University, Aoba-ku, Sendai 980-8577, Japan.

[b]Chemical Materials Development Department, TANAKA PRECIOUS METAL TECHNOLOGIES Co., Ltd., Tsukuba Technical Center, 22 Wadai, Tsukuba, Ibaraki 300-4247, Japan.

[†]These authors contributed equally.

*Correspondence to: das.saikat.c4@tohoku.ac.jp (S.D.), yuichi.negishi.a8@tohoku.ac.jp (Y.N.)

Table of Contents

Materials and Methods

Materials

All reagents and solvents were procured from commercial sources and used as received without additional purification unless otherwise stated. Silver nitrate ($AgNO_3$) was procured from Kanto Chemical Co., Inc. Silver trifluoroacetate (CF_3COOAg), acetonitrile (MeCN), methanol (MeOH), and ethanol (EtOH) were procured from FUJIFILM Wako Pure Chemical Corporation. *tert*-butyl mercaptan, L-lysine, L-arginine, L-aspartic acid, and L-glutamic acid were obtained from Tokyo Chemical Industry Co., Ltd. 3,6-di(4-pyridyl)-1,2,4,5-tetrazine was procured from ET Co., Ltd.

Instrumentation

Single-crystal X-ray diffraction (SCXRD) data were recorded after the single crystal was immersed in the cryoprotectant Parabar 10312 (Hampton Research, 34 Journey, Aliso Viejo, CA 92656-3317 USA) and mounted on a Dual-Thickness MicroMounts™ (MiTeGen, LLC, Ithaca, NY, USA). Diffraction measurements were carried out on a Bruker D8 QUEST diffractometer using monochromated Mo Kα radiation (λ = 0.71073 Å). The crystal structure was solved with the Apex3 Bruker software package.[1] Powder X-ray diffraction (PXRD) patterns were collected using a Rigaku MiniFlex X-ray diffractometer equipped with a CuKα radiation source (λ = 1.5418 Å) and operated at 40 kV and 15 mA. Diffraction patterns were acquired in the 2θ range of 5–40º using a step size of 0.02º and a scanning speed of 2.0º min^{-1}. X-ray photoelectron spectroscopy (XPS) spectra were acquired on a JPS-9-1-MC electron spectrometer (JEOL, Tokyo, Japan) employing Mg K_α radiation (1253.6 eV) as the excitation source. All binding energies were referenced to the neutral C 1s peak at 283.3 eV. Thermal stability of the SCAM was evaluated by thermogravimetric analysis (TGA) using a Thermo plus EVO2 thermal analyzer, with a heating rate of 10 °C min^{-1} from room temperature to 800 °C under a nitrogen flow of 50 mL min^{-1}. Optical micrographs were recorded with an Olympus SZX7 stereo microscope. Scanning electron microscopy/energy-dispersive X-ray spectroscopy (SEM-EDX) measurements were carried out on a JEOL JSM-7800 field emission scanning electron microscope equipped with an Oxford X-Max EDX detector. Nitrogen adsorption-desorption measurements were carried out at 77 K using a Quantachrome Autosorb iQ3 gas sorption analyzer. Before measurement, the sample was

degassed at 50 °C for 8 h under high vacuum generated by a turbomolecular pump. The specific surface area was determined using the multipoint Brunauer–Emmett–Teller (BET) equation applied to the adsorption data. UV-Vis absorption data were obtained on a JASCO V-770 spectrophotometer. Photoluminescence (PL) spectra were recorded using an Edinburgh Instruments (EI) FLS1000 spectrofluorometer equipped with a continuous (450 W) xenon lamp.

Synthesis methods

Synthesis of silver *tert*-butylthiolate (AgS^{t}Bu)

AgS^{t}Bu was synthesized according to a previously reported method.[2,3] Silver nitrate (2.204 g, 12.8 mmol) was stirred in MeCN (30 mL) for 10 min in a 100 mL Erlenmeyer flask. *tert*-butyl mercaptan (5 mL, 44 mmol) was then added, and the reaction mixture was stirred for an additional 15 min, resulting in the formation of a white precipitate. The solid was collected by centrifugation, thoroughly washed with MeOH until the thiol odor disappeared, followed by a final wash with MeCN (40 mL). Vacuum drying overnight yielded AgS^{t}Bu as a white powder in 85% yield.

Synthesis of TUS 9

AgS^{t}Bu (24 mg, 0.12 mmol) was dispersed in a mixed solvent system of MeCN and EtOH (5 mL, 1:1 v/v) under continuous stirring in a glass vial to generate a uniform suspension. CF_3COOAg (24 mg, 0.11 mmol) was then added, and the mixture was stirred until a clear solution was obtained. To this solution, 3,6-di(4-pyridyl)-1,2,4,5-tetrazine (14.2 mg, 0.06 mmol) was introduced. The resulting mixture was gently agitated to ensure uniform dispersion and then left undisturbed at 273 K for 7 days to facilitate slow nucleation and crystal growth. Pink truncated octahedral crystals of **TUS 9** formed on the walls and at the bottom of the vial and were isolated by washing with MeCN and EtOH, affording the product in 76% yield (based on Ag).

Sensing of amino acids

The sensing performance of **TUS 9** toward biologically relevant amino acids was systematically investigated using fluorescence spectroscopy. Finely ground samples of the SCAM (2 mg) were dispersed in 3.0 mL of aqueous solutions containing individual amino acids. The suspensions were subjected to ultrasonic treatment to ensure uniform dispersion and promote interfacial contact between the analytes and the SCAM surface. After sonication, the mixtures were allowed to stand to form stable emulsions, following which fluorescence measurements were carried out. Under these conditions, the **TUS 9** suspensions remained visually stable without noticeable precipitation during the fluorescence measurement period (typically < 1 h). Upon prolonged standing, minor settling may occur due to the particulate nature of the material; however, the sedimentation is fully reversible and the sample can be readily redispersed by gentle shaking or brief sonication without any loss of luminescence response. Four representative amino acids—L-lysine, L-arginine, L-aspartic acid, and L-glutamic acid—were selected as model analytes to evaluate the response behavior of **TUS 9**. To quantitatively assess the concentration-dependent sensing characteristics, fluorescence titration experiments were conducted using aqueous solutions of each amino acid over a range of concentrations. In addition, recyclability tests were performed to examine the operational stability of the SCAM sensor. All sensing experiments were repeated three times independently to ensure reproducibility and statistical reliability. The fluorescence quenching efficiency was calculated using the equation:

$$\text{Quenching efficiency (\%)} = \frac{I_0 - I}{I_0} \times 100$$

where I_0 and I represent the fluorescence intensities of **TUS 9** before and after the addition of the analyte, respectively.

Table S1. Crystal data and structure refinement parameters of **TUS 9**.

Identification code	TUS 9
Empirical formula	$C_{62}H_{104}Ag_{13}F_9N_8O_6S_{10}$
CCDC number	2523357
Formula weight	2951.44
Temperature/K	273.15
Crystal system	Monoclinic
Space group	*C*2/*c*
a/Å	17.536(2)
b/Å	20.071(2)
c/Å	26.605(3)
α/°	90
β/°	102.569(3)
γ/°	90
Volume/Å^3	9139.2(17)
Z	4
ρ_{calc}/g cm^{-3}	2.145
μ/mm^{-1}	3.011
F(000)	5728
Radiation	MoKα (λ = 0.71073)
2Θ range for data collection/°	1.862 to 24.713°
Index ranges	-20<=h<=20, -20<=k<=23, -29<=l<=31
Reflections collected	20652
Independent reflections	7485 [R_{int} = 0.0840]
Data/restraints/parameters	7485/540/559
Goodness-of-fit on F^2	1.005
Final R indexes [I>=2σ (I)]	R1 = 0.0525, wR2 = 0.0996
Final R indexes [all data]	R1 = 0.1025, wR2 = 0.1172
Largest diff. peak/hole / e Å^{-3}	1.456/-1.100

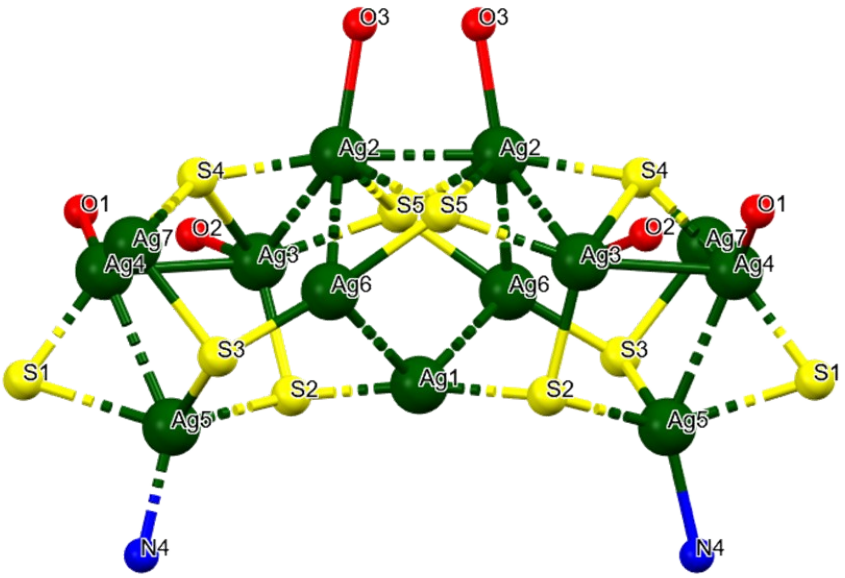

Fig. S1 Labeled depiction of the Ag_{13} nanocluster featuring ten S^{t}Bu and three CF_3COO^- ligands as stabilizing ligands, along with two coordinated linker molecules.

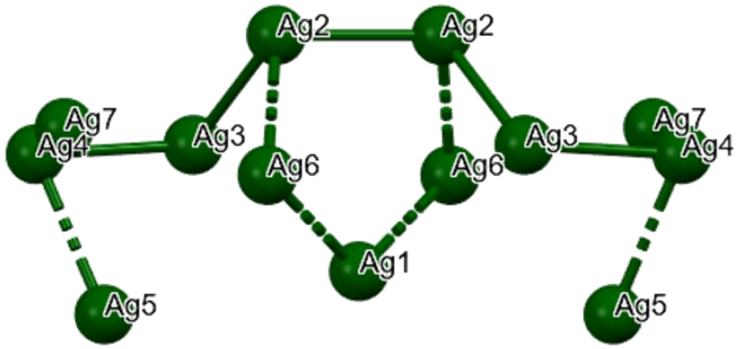

Fig. S2 Labeled Ag_{13} core displaying an arched (bow-shaped) scaffold, featuring a top Ag2–Ag2 dimer forming the "crown" and a basal Ag1 node, with Ag6 units bridging the crown to the base and Ag3–Ag2 connections forming two symmetric lateral wings that define the overall bow-shaped geometry.

Table S2. Summary of Ag−Ag bond distances for the Ag_{13} core structure presented in Fig. S2.

Atom1	Atom2	Bond length / Å		Bond length / Å
Ag1	Ag6	3.065	Maximum	3.275
Ag2	Ag2	2.971	Minimum	2.851
Ag2	Ag3	3.275	Average	3.033
Ag2	Ag6	3.092	S.D.	0.132
Ag3	Ag4	2.851		
Ag4	Ag5	2.968		
Ag4	Ag7	3.007		

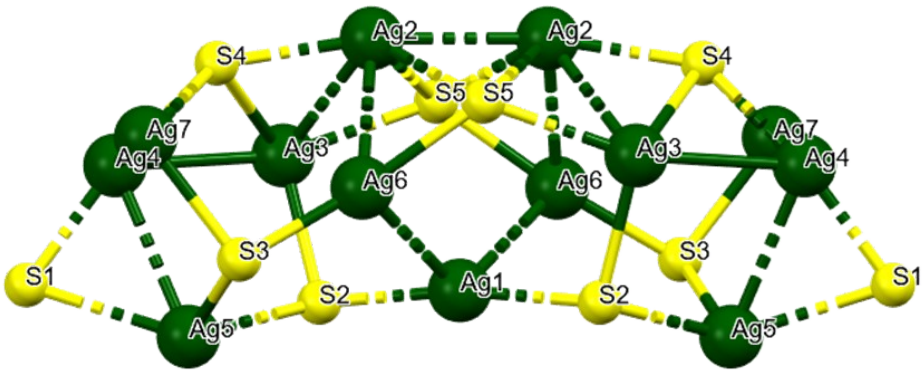

Fig. S3 Binding configuration of the ten thiolate ligands on the Ag_{13} core.

Table S3. Summary of Ag–S bond distances corresponding to Fig. S3.

Atom1	Atom2	Bond length / Å		Bond length / Å
Ag1	S2	2.387	Maximum	2.796
Ag2	S4	2.552	Minimum	2.387
Ag2	S5	2.603	Average	2.561
Ag2	S5	2.762	S.D.	0.135
Ag3	S2	2.506		
Ag3	S4	2.724		
Ag3	S5	2.700		
Ag4	S1	2.410		
Ag4	S4	2.557		
Ag5	S1	2.796		
Ag5	S2	2.574		
Ag5	S3	2.557		
Ag6	S3	2.387		
Ag6	S5	2.399		
Ag7	S1	2.447		
Ag7	S3	2.482		
Ag7	S4	2.691		

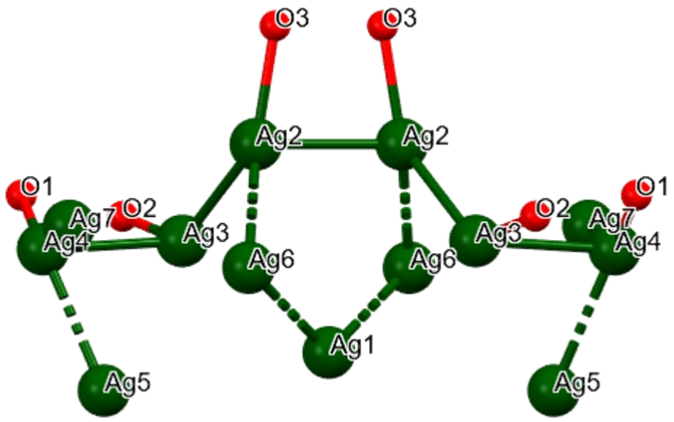

Fig. S4 Attachment pattern of three trifluoroacetate ligands to the Ag_{13} cluster.

Table S4. Summary of Ag–O bond distances corresponding to Fig. S4.

Atom1	Atom2	Bond length / Å		Bond length / Å
Ag2	O3	2.337	Maximum	2.431
Ag3	O2	2.326	Minimum	2.326
Ag4	O1	2.431	Average	2.365
			S.D.	0.058

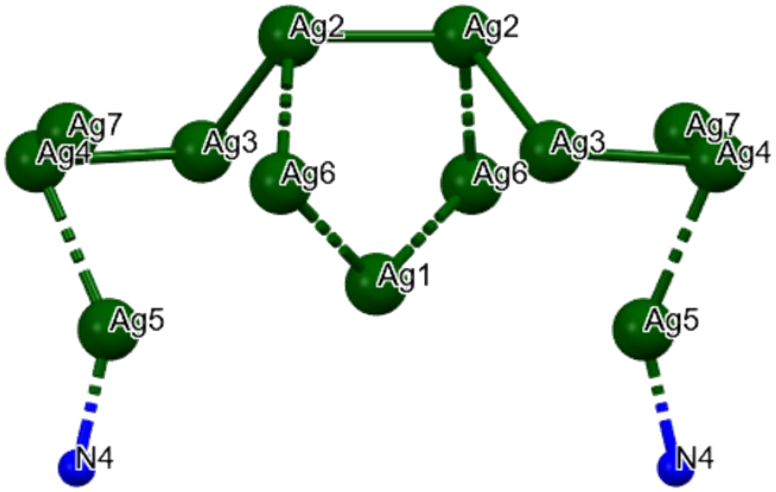

Fig. S5 Attachment pattern of two linker molecules to the Ag_{13} cluster.

Table S5. Summary of Ag–N bond distances corresponding to Fig. S5.

Atom1	Atom2	Bond length / Å		Bond length / Å
Ag5	N4	2.212	Maximum	2.212
			Minimum	2.212
			Average	2.212

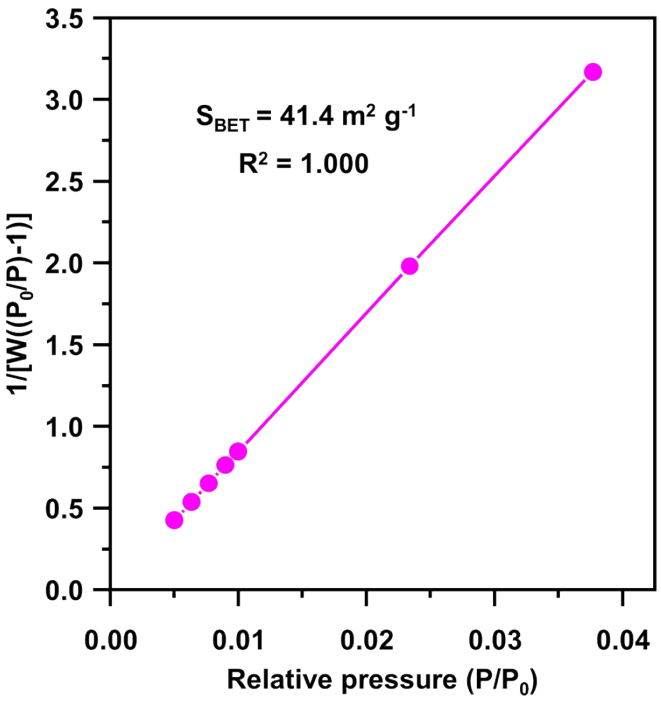

Fig. S6 BET plot of **TUS 9** derived from nitrogen adsorption measurements at 77 K.

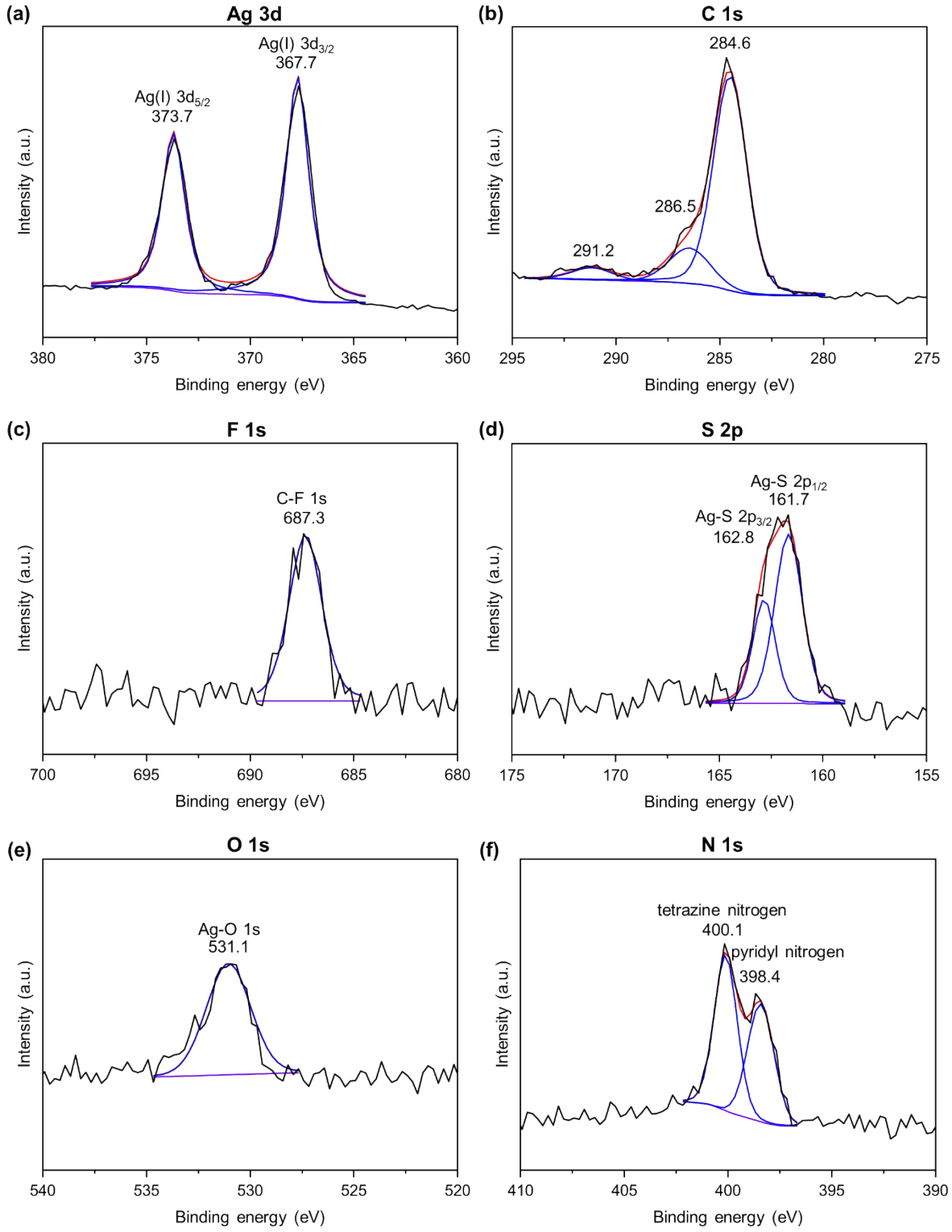

Fig. S7 High-resolution XPS spectra of individual elements in **TUS 9**.

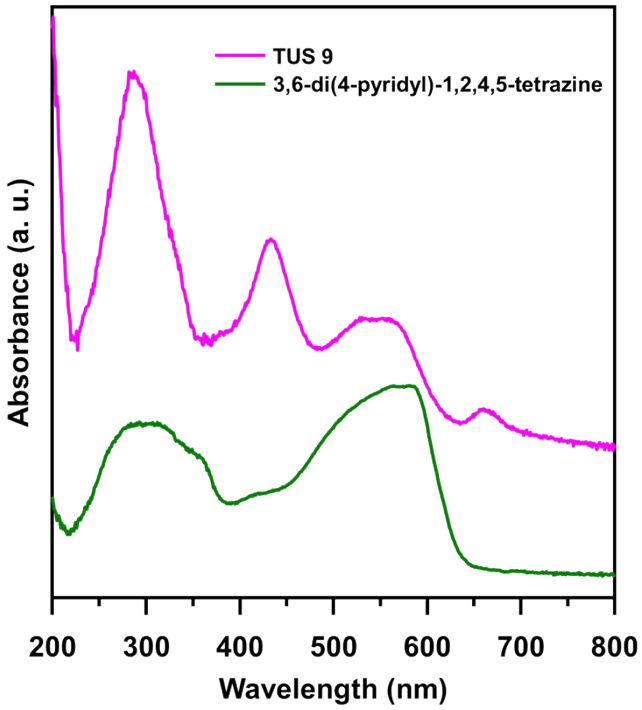

Fig. S8 Solid-state UV-Vis absorbance spectra of **TUS 9** and 3,6-di(4-pyridyl)-1,2,4,5-tetrazine linker.

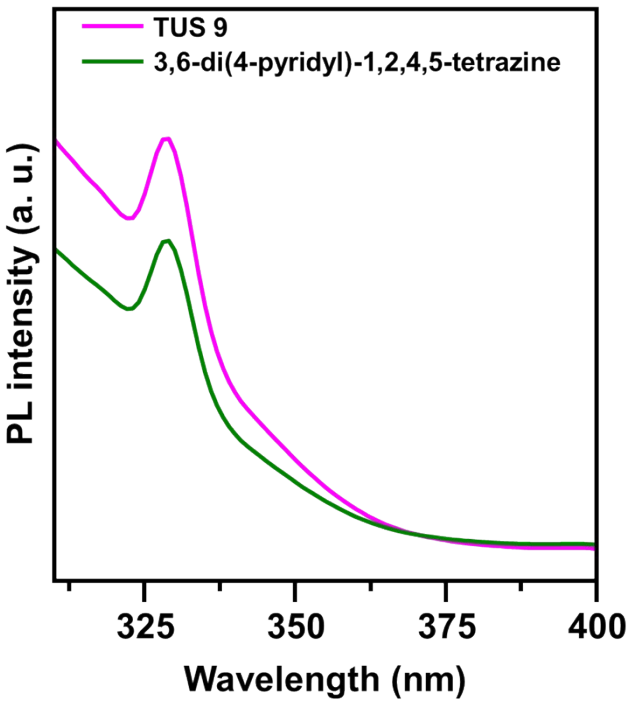

Fig. S9 Comparison of photoluminescence intensity of 3,6-di(4-pyridyl)-1,2,4,5-tetrazine linker and **TUS 9** in solid state at 287 nm excitation.

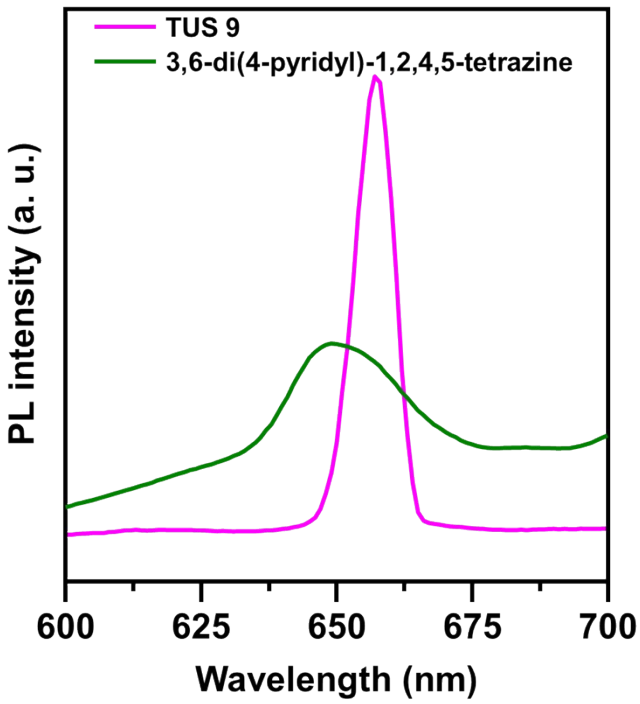

Fig. S10 Comparison of photoluminescence intensity of 3,6-di(4-pyridyl)-1,2,4,5-tetrazine linker and **TUS 9** in solid state at 433 nm excitation.

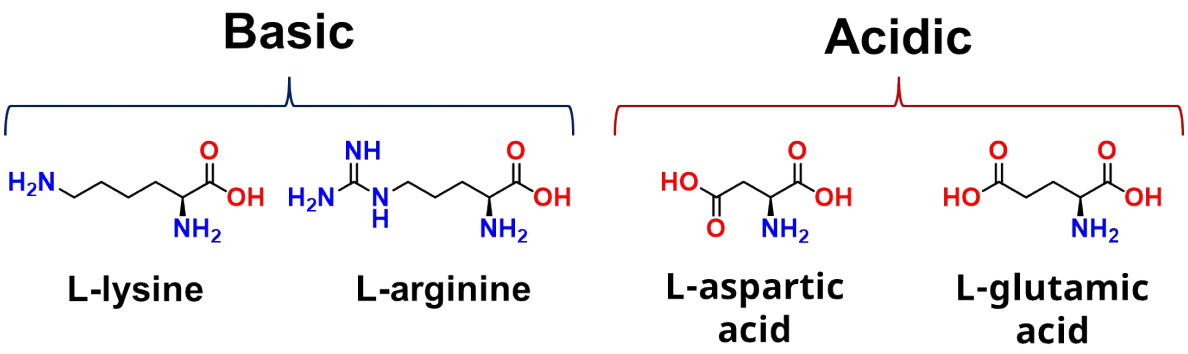

Fig. S11 Chemical structures of the amino acid molecules.

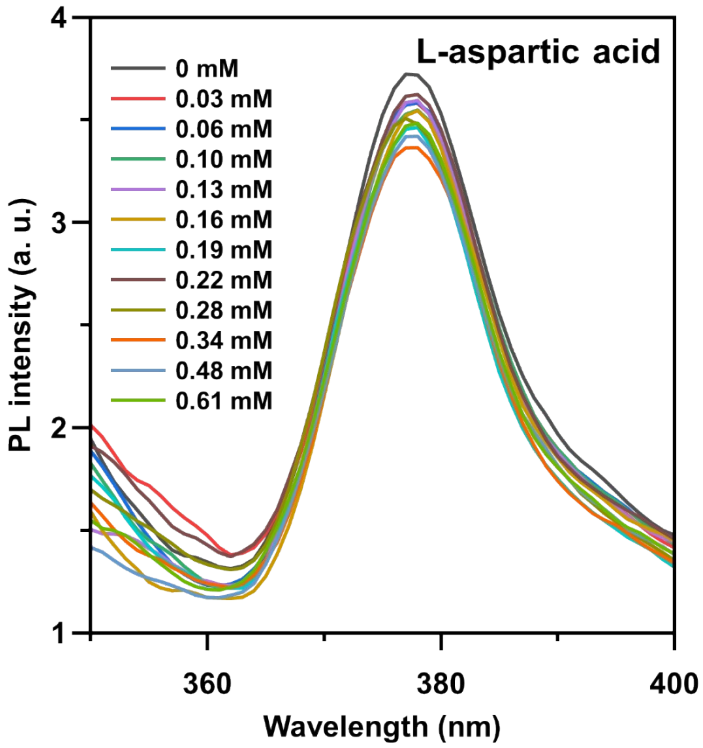

Fig. S12 Photoluminescence response of **TUS 9** as a function of L-aspartic acid concentration.

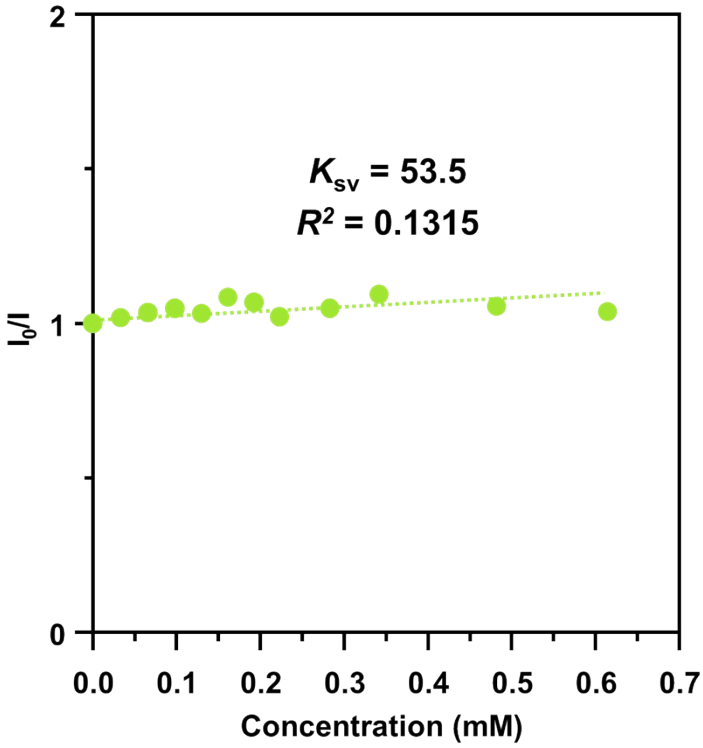

Fig. S13 Stern–Volmer plot illustrating the photoluminescence quenching response of **TUS 9** towards L-aspartic acid in aqueous medium.

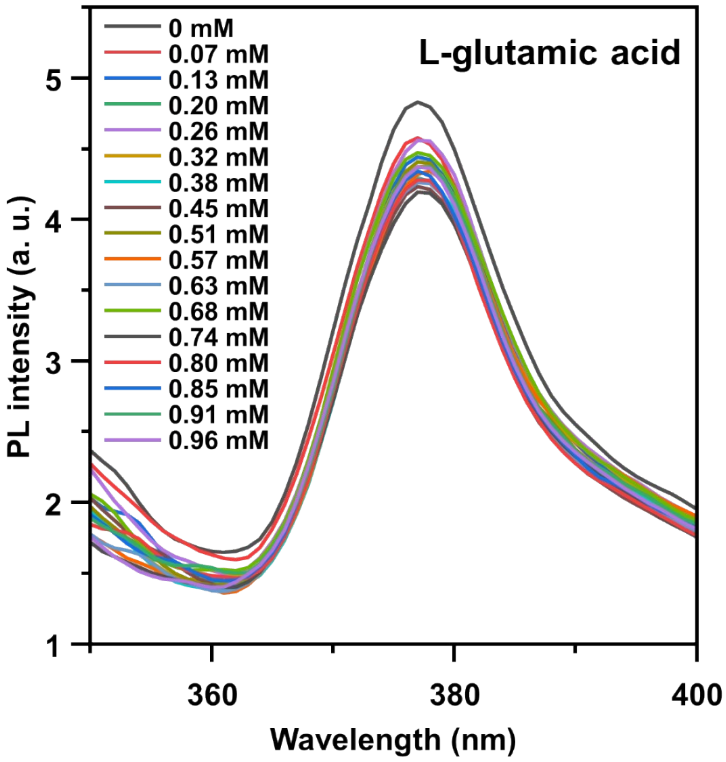

Fig. S14 Photoluminescence response of **TUS 9** as a function of L-glutamic acid concentration.

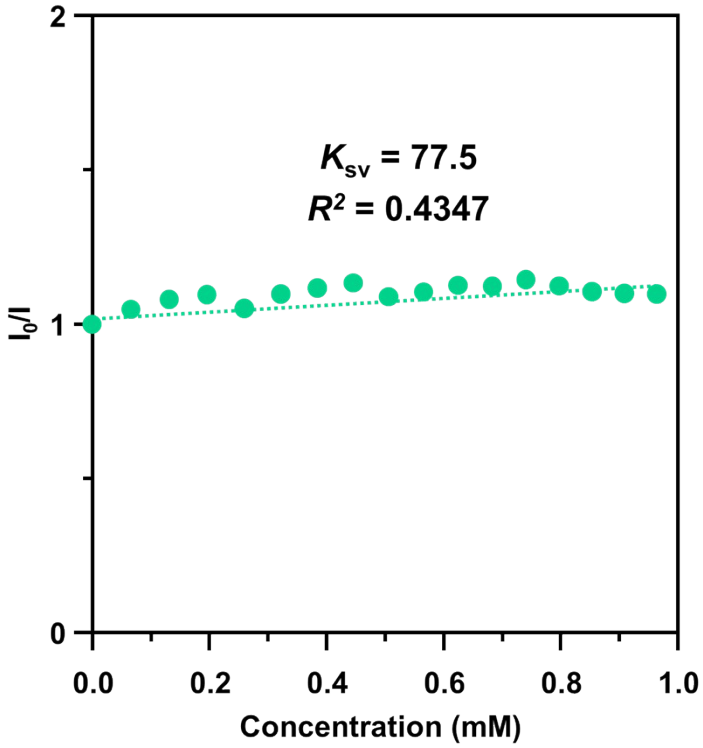

Fig. S15 Stern–Volmer plot illustrating the photoluminescence quenching response of **TUS 9** towards L-glutamic acid in aqueous medium.

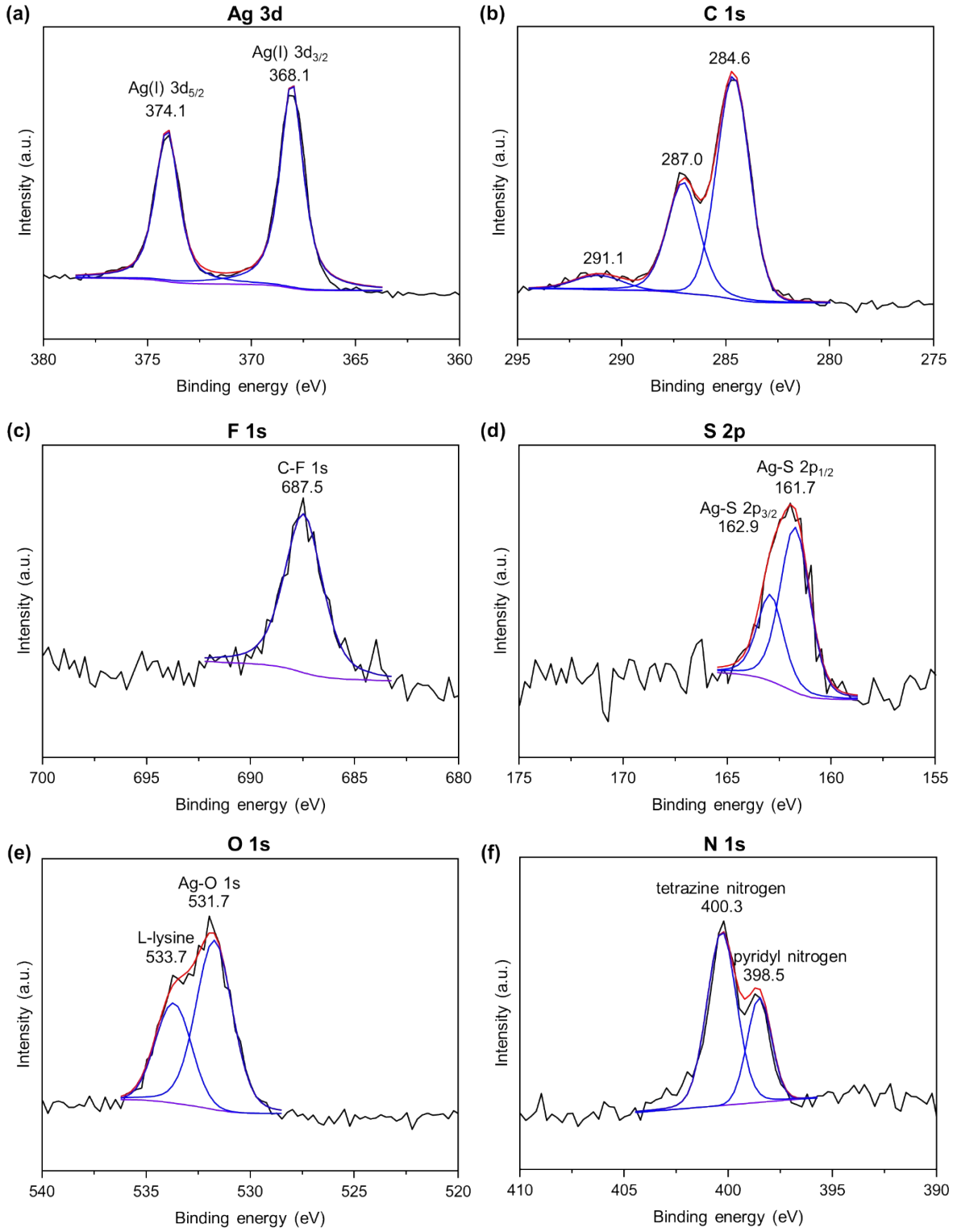

Fig. S16 High-resolution XPS spectra of individual elements in **TUS 9** after sensing L-lysine.

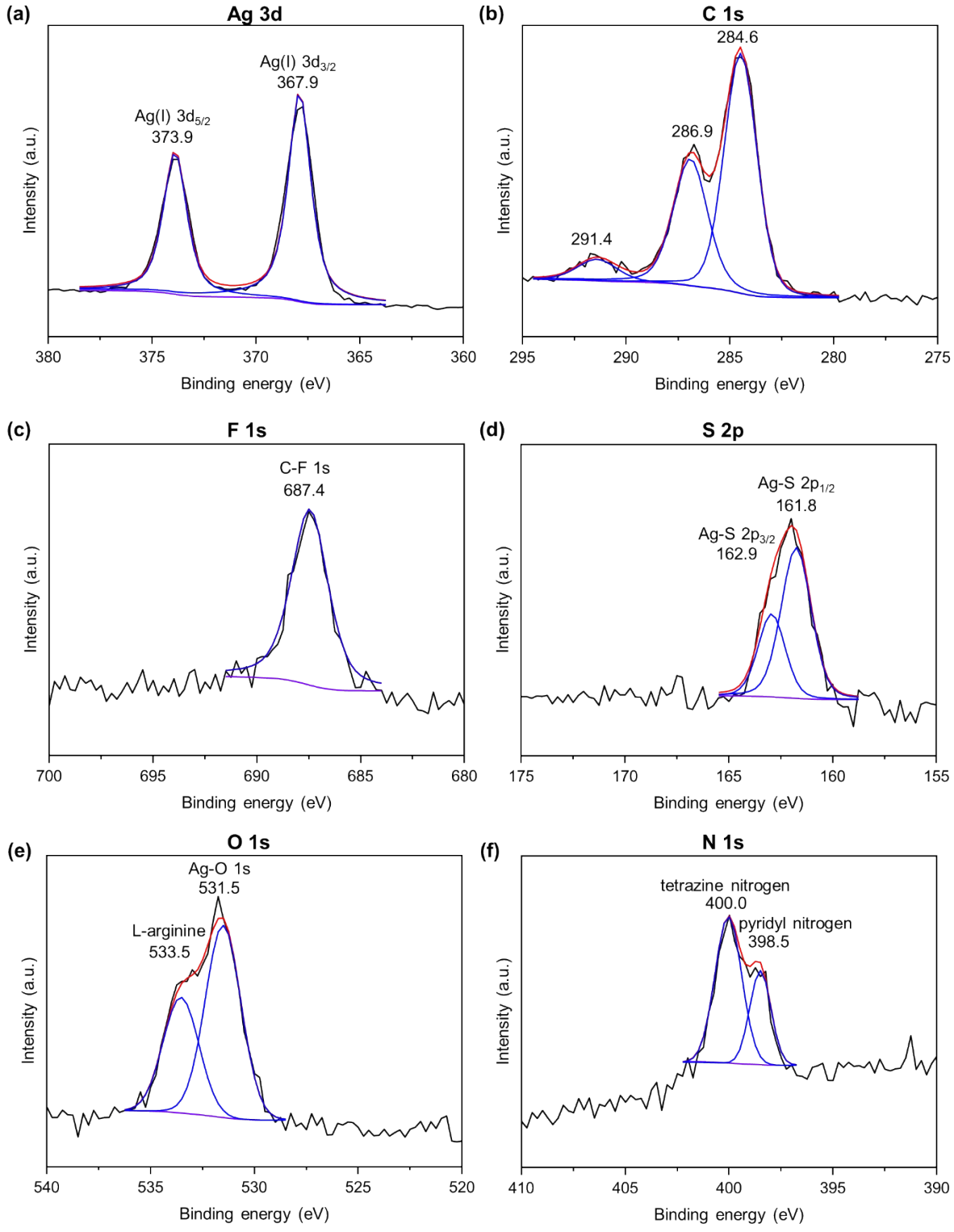

Fig. S17 High-resolution XPS spectra of individual elements in **TUS 9** after sensing L-arginine.

References

1. Bruker APEX3, v2019.1–0, Bruker AXS Inc., Madison, WI, USA, 2019.
2. B. K. Teo, Y. H. Xu, B. Y. Zhong, Y. K. He, H. Y. Chen, W. Qian, Y. J. Deng and Y. H. Zou, *Inorg. Chem.*, 2001, **40**, 6794-6801.
3. S. Das, T. Sekine, H. Mabuchi, S. Hossain, S. Das, S. Aoki, S. Takahashi and Y. Negishi, *Chem. Commun.*, 2023, **59**, 4000-4003.